Int. J. Heat Mass Transfer. Vol. 28, No. 8, pp. 1597–1611, 1985
Printed in Great Britain

0017-9310/85 $3.00 + 0.00
Pergamon Press Ltd.

Natural convection with combined heat and mass transfer buoyancy effects in a porous medium

OSVAIR V. TREVISAN and ADRIAN BEJAN

Department of Mechanical Engineering and Materials Science, Duke University, Durham, NC 27706, U.S.A.

(*Received* 20 *August* 1984 *and in final form* 24 *January* 1985)

Abstract—This paper describes a comprehensive study of the natural convection phenomenon occurring inside a porous layer with both heat and mass transfer from the side. The natural circulation is driven by a combination of buoyancy effects due to both temperature and concentration variations. The first part of the study consists of an extensive series of numerical simulations conducted in the range $0.01 \leqslant Le \leqslant 100$, $50 \leqslant Ra_H \leqslant 10^4$, $-5 \leqslant N \leqslant +3$ and $H/L = 1$, where Le, Ra_H, N and H/L are the Lewis number, Darcy-modified Rayleigh number, buoyancy ratio and geometric aspect ratio of the porous layer. In the second part, the phenomenon is studied based on scale analysis: the chief conclusions of this part, namely, the order-of-magnitude predictions for the overall heat and mass transfer rates and their respective domains of validity, are shown to be in agreement with the results produced by discrete numerical experiments. Furthermore, the scale analysis is used to sort out the many effects that influence the overall heat and mass transfer results of numerical experiments.

1. INTRODUCTION

THE FOCUS of the present study is on the fundamentals of the flow in a porous medium confined between two vertical walls maintained at different temperatures and different concentrations of a certain chemical species (Fig. 1). The novel aspect of this research is the often antagonistic relationship between the two buoyancy effects that drive the flow, namely, the density difference caused by temperature variations and the density difference caused by concentration variations. The engineering applications of this phenomenon are important; for example, the migration of moisture through the air contained in fibrous insulations and grain storage installations, and the dispersion of chemical contaminants through water-saturated soil. Despite these applications, and despite the strong interest expressed by the fluid mechanics community in the same phenomenon in fluids without a porous structure [1], the flow caused by competing buoyancy effects in a vertical porous layer has escaped scrutiny.

In the study of natural convection through porous media, the bulk of the research effort has been devoted to the flow caused by a single buoyancy effect, namely, the effect of temperature variations. The interest in this class of flows has been stimulated by heat transfer engineering applications such as geothermal energy conversion and thermal insulation design [2], hence the two main configurations in which these heat-transfer-driven flows have been studied:

(i) heat transfer across a horizontal porous layer with horizontal walls at different temperatures,
(ii) heat transfer through a layer with different vertical wall temperatures and adiabatic horizontal walls.

For configuration (i), the earliest work [3] showed that, as in the classical Bénard flow problem, convection can occur only above a critical Rayleigh number. Much of the more recent work has been directed at more complex convection onset problems, at finite-amplitude convection at supercritical Rayleigh numbers in homogeneous horizontal layers and, in some cases, in nonhomogeneous layers (see, for example, refs. [4–18]). Some of this literature has been reviewed by Combarnous and Bories [19].

In configuration (ii) with single buoyancy effect, the experiments of Schneider [20], Mordchelles-Regnier *et al.* [21] and Klarsfeld [22] demonstrated that the net heat transfer rate across a vertical layer increases monotonically as the Rayleigh number increases. These measurements were verified later by Bankvall [23] in a numerical study which simulated the steady-state convection pattern. Similar numerical results were obtained by Chan *et al.* [24] and Burns *et al.* [25]. The latter group illustrated also the effect of fluid leakage

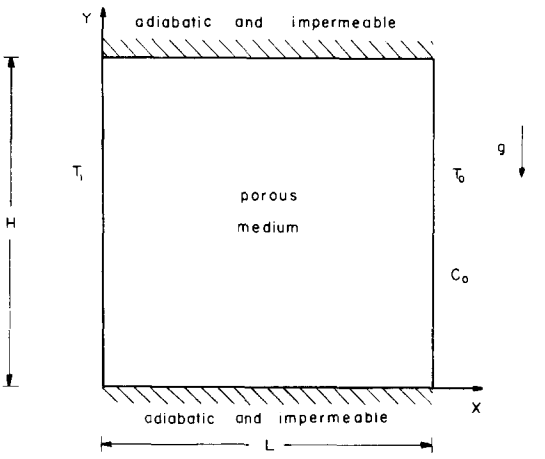

FIG. 1. Schematic of a two-dimensional porous layer subjected to heat and mass transfer in the horizontal direction.

NOMENCLATURE

C	concentration
C_0	concentration of right wall
C_1	concentration of left wall
D	mass diffusivity
g	gravitational acceleration
H	height of porous layer
K	permeability
L	length of porous layer
Le	Lewis number, α/D
N	buoyancy ratio, equation (15)
Nu	Nusselt number, equation (20)
Ra_H	Darcy–Rayleigh number, equation (15)
Sh	Sherwood number, equation (21)
T	temperature
T_0	temperature of right wall
T_1	temperature of left wall
u, v	velocity components
x, y	Cartesian coordinates, Fig. 1.

Greek symbols

α	thermal diffusivity, $k/(\rho c_p)_{fluid}$
β	coefficient of thermal expansion
β_c	coefficient of concentration expansion
δ_c	concentration boundary-layer thickness
δ_T	thermal boundary-layer thickness
ΔC	concentration difference, $C_1 - C_0$
ΔT	temperature difference, $T_1 - T_0$
ν	kinematic viscosity
ρ	density
ψ	streamfunction.

Subscript

*	dimensionless variables.

through the walls which contain the rectangular porous structure; in addition, Burns *et al.* [25] described analytically the convective pattern in the limit of extremely tall layers ($L/H \to 0$). The theoretical work on convection-dominated heat transfer in configuration (ii) was pioneered by Weber [26] who developed an Oseen-linearized solution for the boundary layer regime in a very tall layer ($H/L \gg 1$). The Weber solution was modified to account for the heat transfer which takes place vertically through the core region of moderately tall layers [27]. Simpkins and Blythe [28] reported an alternative theory for the boundary-layer regime, based on an original solution of the integral type [29]. The same authors extended their theory to the more general case where the fluid viscosity is sensitive to temperature changes [30]. A number of relatively recent studies have shown that the flow pattern in a shallow configuration ($H/L < 1$) can differ from that revealed by tall layer studies [31–33].

Relative to the research activity on Darcy flow driven by a single buoyancy effect, the work on convection driven by two buoyancy effects is quite limited, and, with very few exceptions, the work that has been published deals with configuration (i). The linear stability characteristics of the flow in horizontal layers with imposed vertical temperature and concentration gradients has been the subject of studies by Nield [34], Gershuni *et al.* [35] and Turner and Gustafson [36]. With regard to porous layers heated from the side, configuration (ii), the focus has been on the double-diffusive instability of the double boundary-layer structure that forms near a vertical wall immersed in a temperature and concentration stratified porous medium [37]. In a recent study, Raptis *et al.* [38] constructed similarity solutions for the boundary layer near a vertical wall immersed in a porous medium with constant temperature and concentration: this study is based on the assumption that the flow and all of its characteristics are independent of altitude.

Considering the research contributions reviewed above, the objective of the analytical and numerical work presented in this paper is to shed light on an entirely new class of flows in fluid-saturated porous media. The present work covers the previously untraveled territory of flows in configuration (ii) with combined buoyancy effects.

2. MATHEMATICAL FORMULATION

The system considered in this study is the two-dimensional vertical porous layer subjected to a concentration difference ΔC and a temperature difference ΔT in the horizontal direction (Fig. 1). The fluid-saturated porous medium is treated according to the homogeneous model [2] coupled with the Boussinesq approximation that accounts for small density variations due to both temperature and concentration changes at constant pressure. The density variations can be expressed as

$$\rho \cong \rho_0[1-\beta(T-T_0)-\beta_C(C-C_0)] \tag{1}$$

where β and β_C are the coefficients for thermal and concentration expansion,

$$\beta = -\frac{1}{\rho_0}\left(\frac{\partial \rho}{\partial T}\right)_p \tag{2}$$

$$\beta_C = -\frac{1}{\rho_0}\left(\frac{\partial \rho}{\partial C}\right)_p. \tag{3}$$

The equations that account for the conservation of mass, momentum, energy and constituent according to the cited model are [2, 39]

$$\frac{\partial u}{\partial x} + \frac{\partial v}{\partial y} = 0 \tag{4}$$

$$\frac{\partial v}{\partial x}-\frac{\partial u}{\partial y}=\frac{gK}{\nu}\left(\beta\frac{\partial T}{\partial x}+\beta_C\frac{\partial C}{\partial x}\right) \quad (5)$$

$$u\frac{\partial T}{\partial x}+v\frac{\partial T}{\partial y}=\alpha\left(\frac{\partial^2 T}{\partial x^2}+\frac{\partial^2 T}{\partial y^2}\right) \quad (6)$$

$$u\frac{\partial C}{\partial x}+v\frac{\partial C}{\partial y}=D\left(\frac{\partial^2 C}{\partial x^2}+\frac{\partial^2 C}{\partial y^2}\right). \quad (7)$$

In the above equations T represents the local equilibrium temperature of the fluid and the porous matrix, while C is the concentration of the constituent of interest, or, explicitly, the number of kilograms of constituent per unit volume of porous medium (solid and fluid). Symbols g, K, ν represent the gravitational acceleration, the permeability of the porous medium and the kinematic viscosity of the solution contained by the porous matrix. The thermal diffusivity α is defined as the effective thermal conductivity of the saturated porous medium divided by the specific heat capacity of the pure fluid. Parameter D represents the diffusivity of the constituent through the fluid-saturated porous matrix. The boundary conditions sketched on Fig. 1 are

$$u=0,\quad T=T_1,\quad C=C_1 \quad \text{at} \quad x=0 \quad (8)$$

$$u=0,\quad T=T_0,\quad C=C_0 \quad \text{at} \quad x=L \quad (9)$$

$$v=0,\quad \frac{\partial T}{\partial y}=0,\quad \frac{\partial C}{\partial y}=0$$
$$\text{at } y=0 \text{ and } y=H. \quad (10)$$

Equations (4)–(7) may be placed in dimensionless form by introducing the new variables

$$x_*=\frac{x}{L},\quad y_*=\frac{y}{L},\quad \psi_*=\frac{\psi\nu}{gK\beta\Delta TL}$$
$$T_*=\frac{T}{T_1-T_0},\quad C_*=\frac{C}{C_1-C_0} \quad (11)$$

where ψ is the streamfunction ($u=\partial\psi/\partial y$, $v=-\partial\psi/\partial x$). The resulting dimensionless equations are

$$\frac{\partial^2\psi_*}{\partial x_*^2}+\frac{\partial\psi_*^2}{\partial y_*^2}=-\frac{\partial T_*}{\partial x_*}-N\frac{\partial C_*}{\partial x_*} \quad (12)$$

$$\left(\frac{L}{H}\right)Ra_H\left(\frac{\partial\psi_*}{\partial y_*}\frac{\partial T_*}{\partial x_*}-\frac{\partial\psi_*}{\partial x_*}\frac{\partial T_*}{\partial y_*}\right)=\frac{\partial^2 T_*}{\partial x_*^2}+\frac{\partial^2 T_*}{\partial y_*^2} \quad (13)$$

$$\left(\frac{L}{H}\right)Le\,Ra_H\left(\frac{\partial\psi_*}{\partial y_*}\frac{\partial C_*}{\partial x_*}-\frac{\partial\psi_*}{\partial x_*}\frac{\partial C_*}{\partial y_*}\right)=\frac{\partial^2 C_*}{\partial x_*^2}+\frac{\partial^2 C_*}{\partial y_*^2} \quad (14)$$

where

$$N=\frac{\beta_C\Delta C}{\beta\Delta T},\quad Ra_H=\frac{gK\beta\Delta TH}{\alpha\nu},\quad Le=\frac{\alpha}{D} \quad (15)$$

are the buoyancy ratio, the Rayleigh number and the Lewis number. The dimensionless boundary conditions are

$$\psi_*=0,\quad T_*=1,\quad C_*=1 \quad \text{at} \quad x_*=0 \quad (16)$$

$$\psi_*=0,\quad T_*=0,\quad C_*=0 \quad \text{at} \quad x_*=1 \quad (17)$$

$$\psi_*=0,\quad \frac{\partial T_*}{\partial y_*}=0,\quad \frac{\partial C_*}{\partial y_*}=0$$
$$\text{at } y_*=0 \text{ and } y_*=\frac{H}{L}. \quad (18)$$

The natural convection problem formulated above was solved in two ways, first on the basis of discrete numerical experiments (sections 3, 4) and, second, based on order-of-magnitude reasoning (section 5). This balanced approach to studying the combined buoyancy effects in porous medium natural convection eliminates the need for exhaustive numerical simulations and, at the same time, highlights the true scales and 'physics' of the phenomenon.

3. NUMERICAL EXPERIMENTS

Equations (12)–(14) were discretized using the control volume formulation developed by Patankar [40]. The power law scheme was used to calculate both the heat and mass fluxes across the boundaries of each control volume. The simultaneous algebraic equations were solved using an iterative point-by-point method and relaxation parameters. The process was repeated until the changes in ψ_*, T_* and C_* between two successive iterations satisfied the criterion

$$\frac{\sum_{i,j}|\tau_{new}-\tau_{old}|}{\sum_{i,j}|\tau_{new}|}<Res \quad (19)$$

where τ stands for ψ_*, T_* or C_*, while Res is a number sufficiently small so that the overall heat and mass transfer rates calculated at $x_*=0$ and at $x_*=1$ are nearly the same,

$$Nu=\frac{L}{H}\int_0^{H/L}\left(\frac{\partial T_*}{\partial x_*}\right)_{x_*=\xi}dy_*,\quad \xi=0,1 \quad (20)$$

$$Sh=\frac{L}{H}\int_0^{H/L}\left(\frac{\partial C_*}{\partial x_*}\right)_{x_*=\xi}dy_*,\quad \xi=0,1. \quad (21)$$

The difference between the (Nu, Sh) values evaluated at $\xi=0$ and $\xi=1$ was used as an additional check on the convergence of the numerical solution. In all the cases documented by the present study the absolute value of the error parameter

$$Err=\frac{(Nu,Sh)_{\xi=1}-(Nu,Sh)_{\xi=0}}{(Nu,Sh)_{\xi=1}+(Nu,Sh)_{\xi=0}} \quad (22)$$

was maintained below 1%, in order to avoid false convergence in cases where under-relaxation was needed.

The two-dimensional domain of Fig. 1 was covered with an array of $(m-2)\times(n-2)$ square control

Table 1. Grid fineness test ($Le = 1$, $N = 0$, $H/L = 1$, $\alpha = 1$)

Case	Grid fineness ($m \times n$)	Time per iteration CPUs	Nu equation (20)	Nu error equation (22) (%)
$Ra_H = 50$	12×12	0.179	2.24	0.91
$Res = 10^{-4}$	16×16	0.357	2.13	1.31
	22×22	0.730	2.06	1.81
$Ra_H = 50$	12×12	0.173	2.242	0.10
$Res = 10^{-5}$	22×22	0.698	2.059	0.16
	32×32	1.530	2.017	0.31
	42×42	2.694	2.002	0.40
$Ra_H = 2000$	12×12	0.173	12.859	0.07
$Res = 10^{-5}$	22×22	0.684	23.316	0.05
	32×32	1.535	27.104	0.06
	42×42	2.728	27.599	0.06

volumes. The four boundaries were covered with control volumes of zero thickness. In order to properly select the mesh size, the influence of the mesh size on the final solution was tested through the series of runs summarized in Table 1. Varying the grid fineness from 12×12 to 42×42, it became clear that the 32×32 mesh is adequate in the range $(H/L)^2 Ra_H < 5000$ and $(H/L)^2 Ra_H Le\,|N| < 5000$. The results reported in this paper were obtained using the 32×32 grid when parameters $(H/L)^2 Ra_H$ and $(H/L)^2 Ra_H Le\,|N|$ were lower than 5000. In the few cases where these parameters exceed 5000, the grid fineness was improved up to 52×52.

Table 1 shows also the effect of the residue parameter Res on the accuracy of the converged solution. Although the $Res = 10^{-5}$ criterion demands approx. 40% more iterations than the $Res = 10^{-4}$ criterion, the numerical solutions presented in this report were all obtained using $Res = 10^{-5}$. This convergence criterion insured a better than 1% agreement between the overall heat and mass transfer calculations obtained along the two vertical side walls, $\xi = 0$ and $\xi = 1$, equations (20)–(22).

An additional test of the accuracy of the numerical procedure employed in present study is presented in Fig. 2. The present calculations for heat transfer rates in the absence of buoyancy due to concentration gradients are in excellent agreement with heat transfer results published previously [31].

4. MASS AND HEAT TRANSFER RESULTS

An important feature of the natural convection driven by combined buoyancy effects is the diversity of

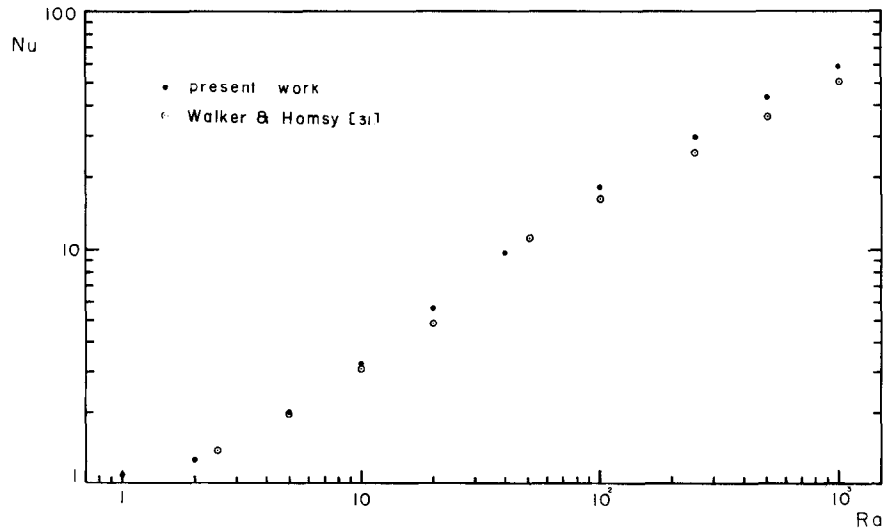

FIG. 2. Numerical accuracy test: comparison between the present results for pure heat transfer ($N = 0$, $H/L = 1$) and results published previously.

the flow regimes that are possible in the configuration of Fig. 1. The large number of possible flows is due to the relatively large number of dimensionless parameters that govern the phenomenon, namely, the Rayleigh number (Ra_H), the Lewis number (Le), the buoyancy ratio (N) and the geometric aspect ratio (H/L). The numerical solutions obtained in this study were designed to assess the effect of each of these dimensionless parameters. In the same sense, the purpose of the scale (order-of-magnitude) analysis presented in the next section is to describe these effects analytically and to sort out the flow regimes that can exist in the porous layer.

As pointed out at the start of the scale analysis of section 5, the natural convection flows under consideration may be divided into two limiting classes, (1) heat-transfer-driven flows, i.e. flows dominated by the buoyancy effect due to temperature changes, and (2) mass-transfer-driven flows where the buoyancy effect is dominated by density changes associated with concentration variations. In the first series of numerical solutions obtained in this study, and summarized in Table 2, we investigated the influence of Ra_H and Le in heat-transfer-driven flows. In this class of flows the buoyancy ratio N is zero: this means that the temperature field is coupled to the flow field and not coupled to the concentration field.

The concentration field depends on both tempera-

Table 2. Summary of numerical experiments on heat-transfer-driven flows ($N = 0$, $H/L = 1$)

Ra_H	Le	T-relaxation factor, α_T	Nu equation (20)	C-relaxation factor, α_C	Sh equation (21)
50	0.01	1.0	2.02	1.0	1.00
50	0.10	1.0	2.02	1.0	1.02
50	0.30	1.3	2.02	1.0	1.13
50	1.00	1.5	2.02	1.2	2.02
50	3.00	1.2	2.02	1.2	4.64
50	10.0	1.5	2.02	1.2	9.69
50	30.0	1.1	2.02	1.0	17.84
50	100.0	1.4	2.00	1.0	31.88
100	0.01	1.0	3.27	1.5	1.00
100	0.10	1.5	3.27	1.2	1.04
100	0.30	1.2	3.27	1.4	1.35
100	1.0	1.5	3.27	1.2	3.27
100	3.0	1.2	3.27	1.0	7.63
100	10.0	1.0	3.27	1.2	15.61
100	30.0	1.2	3.27	1.0	25.99
200	0.01	1.5	5.61	1.2	1.00
200	0.03	1.0	5.61	1.3	1.01
200	0.10	1.5	5.61	1.2	1.12
200	0.30	1.0	5.61	1.4	1.87
200	1.0	1.5	5.61	1.5	5.61
200	3.0	1.2	5.61	1.0	12.52
200	10.0	1.0	5.61	1.0	23.23
200	30.0	1.3	5.37	1.0	37.30
400	0.01	1.2	9.69	1.5	1.00
400	0.10	1.2	9.69	1.5	1.29
400	0.30	1.0	9.69	1.1	2.96
400	1.0	1.2	9.69	1.0	9.69
400	3.0	1.0	9.69	1.1	19.36
400	10.0	1.0	9.69	1.0	30.73
1000	0.1	1.2	18.38	1.2	1.91
1000	0.3	1.1	18.38	1.1	6.22
1000	1.0	1.1	18.38	1.1	18.38
2000	0.03	1.0	27.10	1.3	1.23
2000	0.1	1.0	27.10	1.0	3.11
2000	0.3	1.0	27.10	1.1	11.16
4000	0.03	0.7	35.01	1.1	1.62
4000	0.1	0.7	35.01	1.0	5.90
4000	0.3	0.7	35.01	1.0	19.33
10	1.0	1.1	1.08	1.1	1.08
20	1.0	1.1	1.27	1.1	1.27
2500	1.0	1.1	29.98	1.1	29.98
5000	1.0	0.7	42.87	0.7	42.87
10000	1.0	0.7	58.41	0.7	58.41

Table 3. Summary of numerical experiments on the effect of buoyancy ratio ($Ra_H = 200$, $H/L = 1$)

Le	N	C-relaxation factor, α_C	Sh equation (21)	Sh_{Err} equation (22) (%)	T-relaxation factor, α_T	Nu equation (20)	Nu_{Err} equation (22) (%)
	−3.00	1.0	39.71	0.24	1.2	4.20	0.95
	−2.00	1.0	26.67	0.03	1.2	2.60	0.21
	−1.50	1.0	18.37	0.05	1.2	1.75	0.24
	−1.30	1.1	14.30	0.42	1.2	1.57	0.10
$Le = 10$	−1.15	1.1	11.28	0.01	1.2	1.51	0.11
	−1.00	1.0	7.50	0.24	1.2	1.45	0.20
	−0.85	0.6	8.63	0.79	1.1	3.09	0.08
	−0.70	0.8	11.22	0.05	1.1	3.60	0.02
	−0.50	1.0	15.02	0.20	1.1	4.21	0.01
	+0.50	1.0	28.99	0.10	1.1	6.70	0.03
	+1.00	1.0	32.68	0.10	1.1	8.40	0.05
	+2.00	1.0	36.47	0.09	1.1	11.17	0.05
	−5.0	1.1	15.92	0.04	1.1	15.92	0.04
	−4.0	1.1	13.07	0.04	1.1	13.07	0.04
$Le = 1$	−3.0	1.0	9.69	0.05	1.2	9.69	0.06
	−2.0	1.4	5.61	0.02	1.2	5.61	0.10
	−1.5	1.2	3.27	0.12	1.3	3.26	0.11
	−1.0	1.2	1.00	0.08	1.3	1.0	0.01
	−5.0	1.1	3.02	0.03	1.2	13.29	0.11
	−3.0	1.1	2.04	0.04	1.1	8.15	0.11
$Le = 0.1$	−2.0	1.1	1.54	0.12	1.2	5.24	0.26
	−1.0	1.1	1.00	0.34	1.1	1.00	0.34
	+1.0	1.1	1.44	0.42	1.0	8.95	0.04
	+3.0	1.1	2.48	0.13	1.1	13.76	0.05

ture and flow fields, as indicated by equations (12)–(14). The difference between the concentration and temperature fields is dictated by the Lewis number, in other words, the T and C fields are identical only in the special case $Le = 1$. In addition to the expected relationship between Ra_H and Nu (see also Fig. 2), Table 2 shows that when Ra_H is fixed the Sherwood number consistently increases as the Lewis number increases. In other words, when the heat-transfer-driven flow is fixed, the concentration boundary layers become increasingly thinner as Le increases.

Table 3 summarizes the series of experiments designed to document the effect of buoyancy ratio, N. A bird's-eye view of the trend revealed by these numerical results is conveyed by Fig. 3. The most striking feature of the N effect is the suppression of convection as a

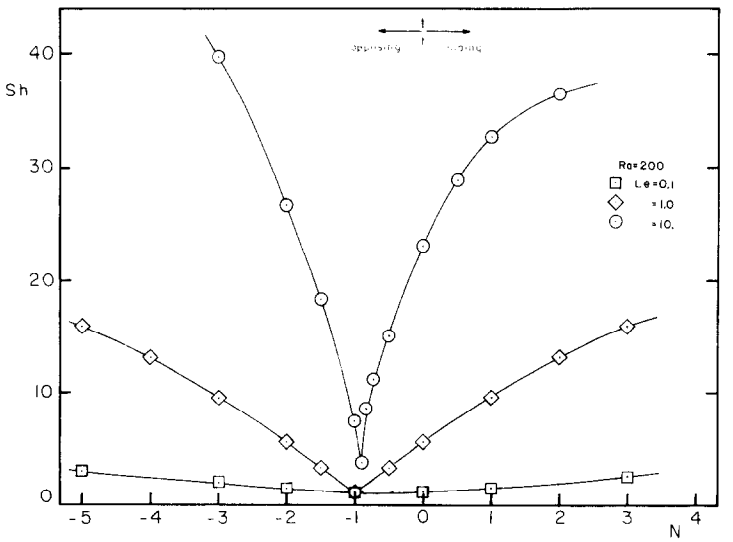

FIG. 3. The effect of buoyancy ratio (N) on overall mass transfer across a porous layer with combined buoyancy effects ($Ra_H = 200$, $H/L = 1$; further numerical details are listed in Table 2).

transport mechanism: the suppression is most dramatic in the vicinity of $N = -1$, that is, in flows where the temperature and concentration buoyancy effects are of the same order of magnitude and in opposite directions. Indeed, the flow disappears altogether in the limiting case $Le = 1$, $N = -1$ [note that when the T and C fields are identical, $N = -1$ causes the RHS of the momentum equation (12) to vanish].

When the Lewis number is not equal to 1, the passage of N through the $N = -1$ range is not accompanied by the total disappearance of the flow. This aspect is illustrated by the sequence of streamlines, isotherms and concentration lines displayed in Fig. 4. The case presented in Fig. 4 corresponds to the boundary-layer regime when N is sufficiently different than -1; furthermore, the Lewis number is equal to 10, which means that in the boundary-layer regime the concentration boundary layers are thinner than the temperature boundary layers.

Figure 4(a) shows that for N values algebraically greater than $N = -0.85$ the natural convection pattern resembles what one would expect in a porous layer in which the opposing buoyancy effect is not the dominant driving force. The flow proceeds clockwise, and the T and C boundary layers start from the lower left-hand and upper right-hand corners. The circulation is reversed at N values as low as $N = -3.0$ as shown in Fig. 4(e); here the flow is mainly counterclockwise, and the boundary layers start from the upper left-hand and lower right-hand corners. The switch from the flow of Fig. 4(b) to that of Fig. 4(d), i.e. the transition to flows dominated by the opposing buoyancy effect, takes place rather abruptly around $N = -0.90$, as shown in Fig. 4(c). During transition, the flow consists primarily of two sluggish cells that fill the entire porous layer. The core, which exhibited temperature and concentration stratification at N values sufficiently above and below -0.90, is now dominated by nearly vertical T and C lines. This last feature is consistent with the tendency of both Nu and Sh to approach the pure diffusion limit (see the V-shaped curves of Fig. 3).

5. SCALE ANALYSIS

In view of the many dimensionless groups that govern the natural convection phenomenon, the order-of-magnitude analysis of the flow promises to be as complicated as the task of selecting the 'best' cases for direct numerical simulation. For this reason it is helpful to *structure* the scale analysis: one way to do this is to recognize from the very start two important extremes in which the phenomenon can exist, namely:

(1) Heat-transfer-driven flows, which are dominated by the buoyancy effect due to side heating,

$$|\beta \Delta T| \gg |\beta_C \Delta C|. \tag{23}$$

(2) Mass-transfer-driven flows, where the buoyancy

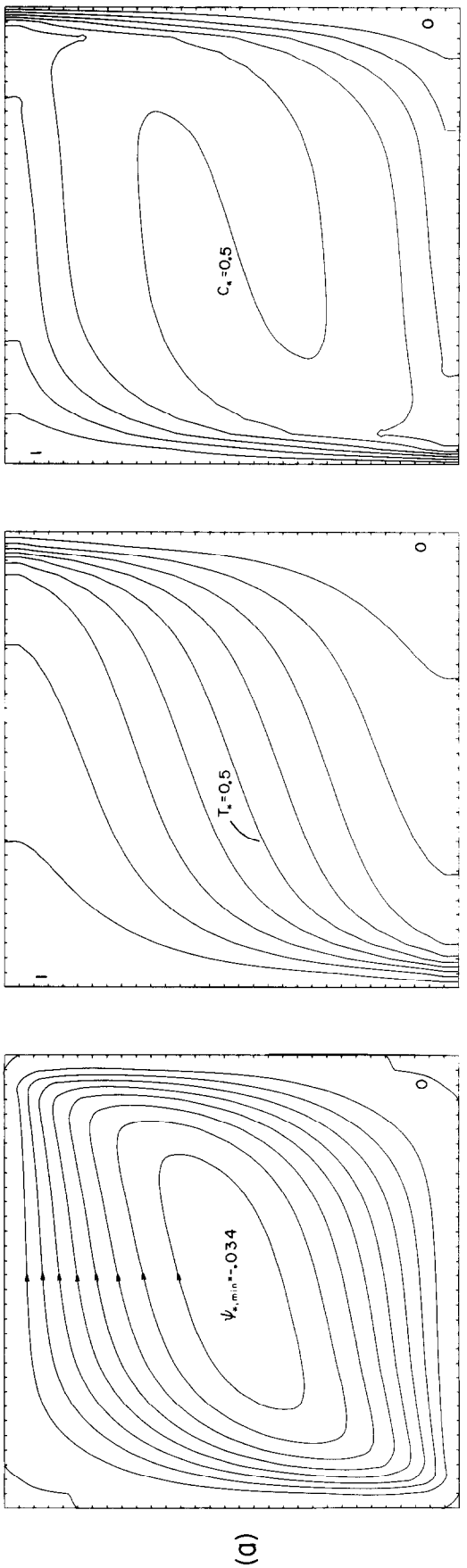

FIG. 4. Patterns of streamlines, isotherms and concentration lines, showing the flow reversal that occurs near $N = -1$ ($Ra_H = 200$, $Le = 10$, $H/L = 1$).(a) $N = -0.50$;(b) $N = -0.85$;(c) $N = -0.90$;(d) $N = -1.50$;(e) $N = -3.0$.

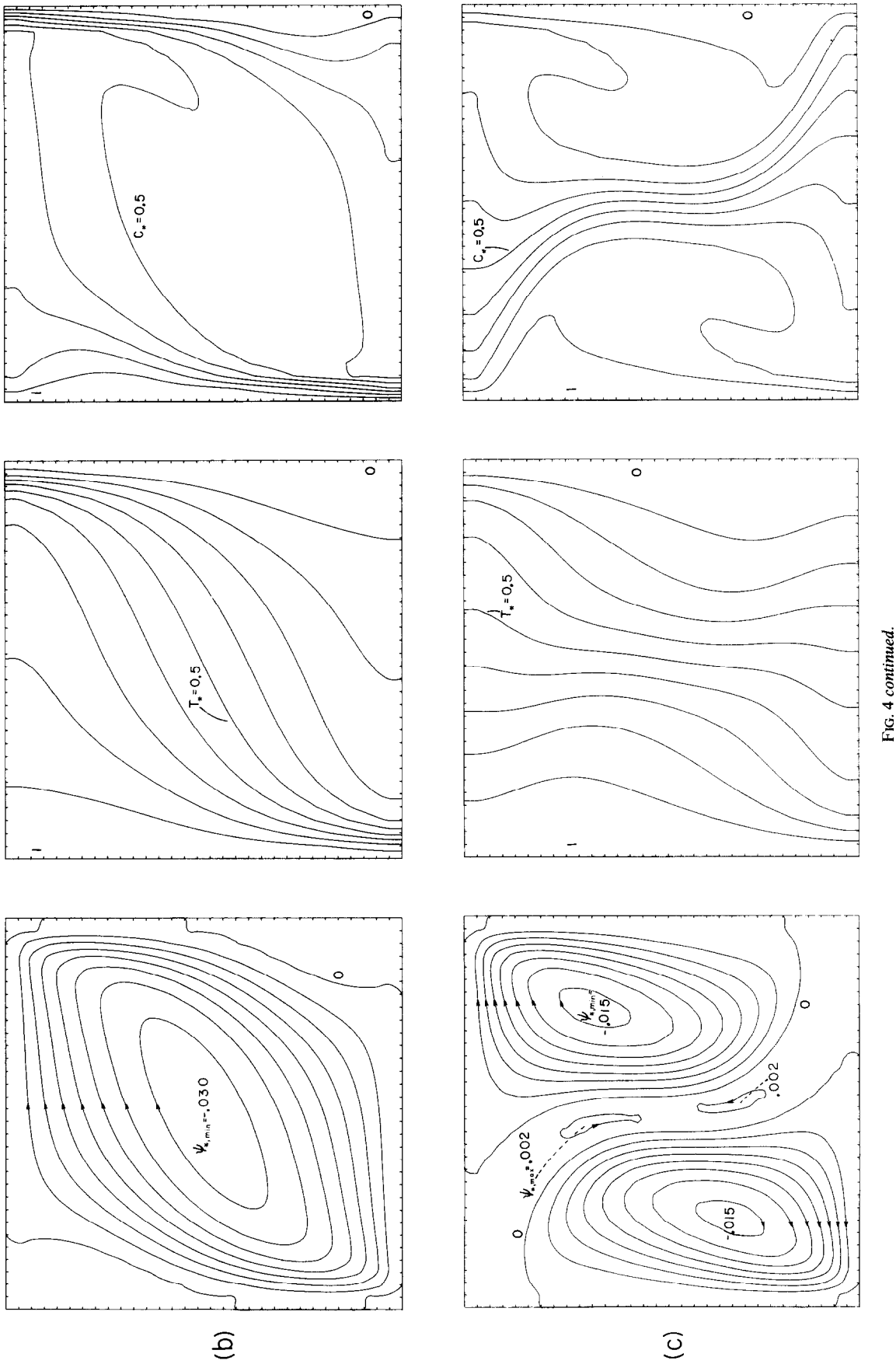

FIG. 4 *continued.*

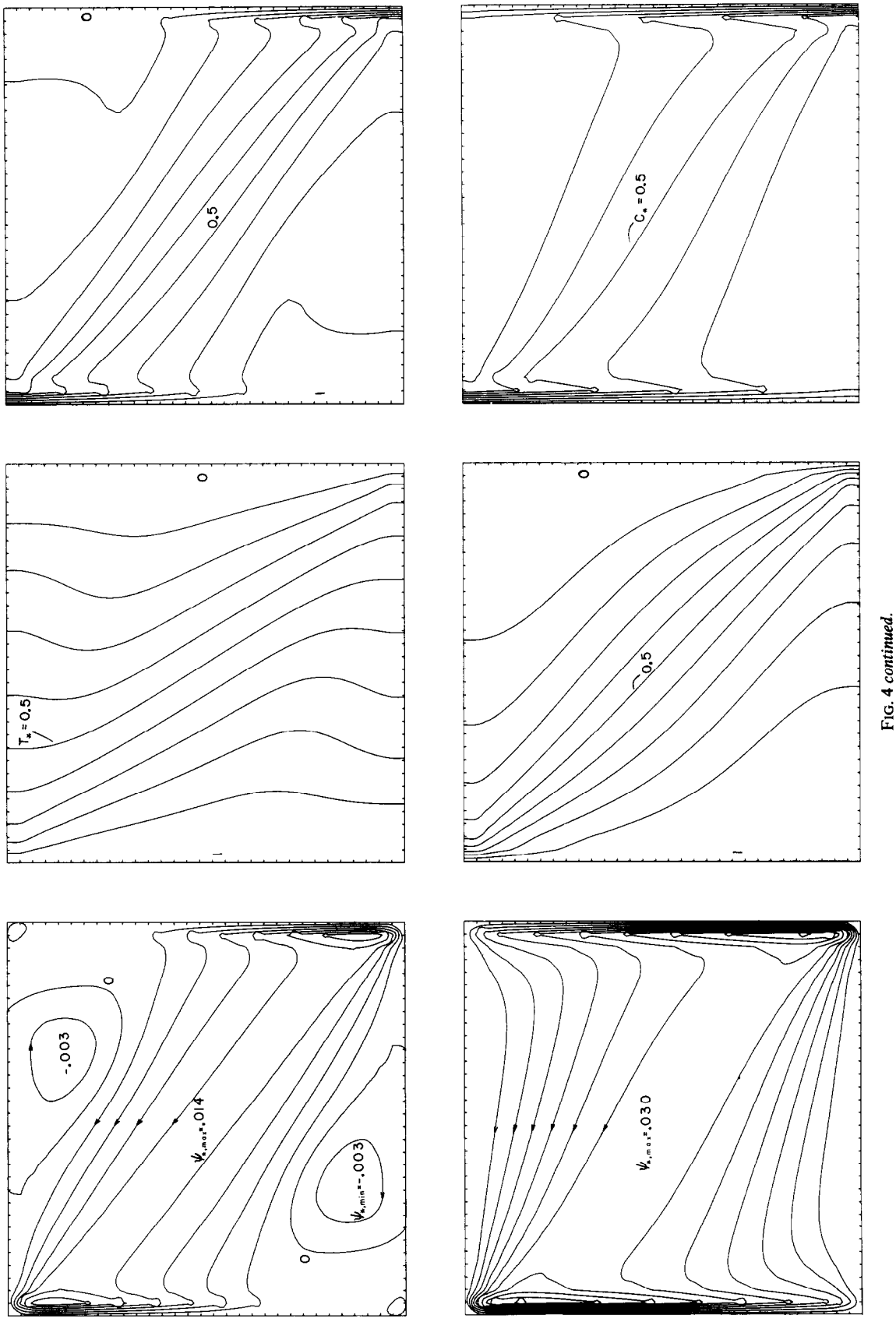

FIG. 4 *continued.*

effect is caused primarily by concentration variations,

$$|\beta\Delta T| \ll |\beta_C \Delta C|. \tag{24}$$

It is worth keeping in mind that parameters β, ΔT, β_C and ΔC can be positive or negative, and that it is only their absolute values that enter in the order-of-magnitude discussion presented below. Thus the absolute value notation '| |' is omitted from the scale analysis. The transition from flows of class (1) to flows of class (2) is dominated by the buoyancy ratio parameter encountered earlier,

$$N = \frac{\beta_C \Delta C}{\beta \Delta T}. \tag{25}$$

Below, we examine separately the most basic scales that characterize the natural convection phenomenon in the two extremes represented by equations (23) and (24).

1. *Heat-transfer-driven flows*

Within class 1, the circulation may feature distinct thermal boundary layers (case 1.1) or a thermal diffusion effect that is felt throughout the layer of thickness L (case 1.2).

Case 1.1. The scale equivalences recommended by the mass, momentum and energy equations in a vertical thermal boundary-layer region of thickness δ_T and height H are, in order,

$$\frac{u}{\delta_T} \sim \frac{v}{H} \tag{26}$$

$$\frac{v}{\delta_T} \sim \frac{gK}{\nu}\beta\frac{\Delta T}{\delta_T} \tag{27}$$

$$v\frac{\Delta T}{H} \sim \alpha\frac{\Delta T}{\delta_T^2}. \tag{28}$$

Solving the above system for the three unknown scales (u, v, δ_T) yields

$$u \sim \frac{\alpha}{H} Ra_H^{1/2} \tag{29}$$

$$v \sim \frac{\alpha}{H} Ra_H \tag{30}$$

$$\delta_T \sim H\, Ra_H^{-1/2} \tag{31}$$

where Ra_H is the usual Darcy-modified Rayleigh number based on height, $Ra_H = Kg\beta H\Delta T/(\alpha\nu)$. Case 1.1 holds as long as the vertical boundary layers are distinct, which means $\delta_T \ll L$ or

$$\frac{L}{H} Ra_H^{1/2} \gg 1. \tag{32}$$

The scale of the concentration boundary-layer thickness δ_C (hence, the mass transfer rate scale) depends on the relative size of δ_C and δ_T. In order to see this, it is helpful to integrate equation (7) across the concentration boundary layer, i.e. from the side wall into the core region where the concentration field C_∞ is mainly a function of altitude (examine the C lines of Fig. 4, at N values sufficiently greater or smaller than the -1 range). We obtain

$$\frac{d}{dy}\int_0^\infty v(C - C_\infty)\,dx = -D\left(\frac{\partial C}{\partial x}\right)_{x=0} \tag{33}$$

which states that the lateral diffusion of constituent into the δ_C-thick layer is equal to the increase in the constituent flowrate upward through the same layer. In an order of magnitude sense, equation (33) reads

$$\frac{1}{H} v\Delta C x_{scale} \sim D\frac{\Delta C}{\delta_C} \tag{34}$$

where x_{scale} is the transversal length scale of the vertical stream of constituent. In order to determine x_{scale} we must recognize that the stream that carries the constituent contains moving fluid and, at the same time, must contain fluid with a high concentration of constituent. In heat-transfer-driven flows the velocity boundary layer is δ_T-thick, and the concentration boundary layer is δ_C-thick. Therefore, the vertical boundary-layer region that houses the constituent stream has a thickness $x_{scale} \sim \min(\delta_T, \delta_C)$: only in this region the fluid flows vertically and, at the same time, has a high concentration of constituent.

The conclusion of the above argument is that in order to determine the δ_C scale from equation (34) we must consider separately the two possibilities, $\delta_C < \delta_T$ and $\delta_C > \delta_T$.

(a) $\delta_C < \delta_T$. In this subcase $x_{scale} \sim \delta_C$, and equation (34) yields

$$\delta_C \sim H(Le\, Ra_H)^{-1/2}. \tag{35}$$

This concentration boundary-layer thickness scale is valid provided δ_C is smaller than δ_T, which via equations (31) and (35) translates into the validity criterion

$$Le \gg 1. \tag{36}$$

(b) $\delta_C > \delta_T$. Using $x_{scale} \sim \delta_T$ in equation (34) we obtain

$$\delta_C \sim H\, Le^{-1}\, Ra_H^{-1/2} \tag{37}$$

which is valid in the remainder of the Le domain, namely $Le \ll 1$. Note further that although the thermal boundary layer has been assumed to be distinct ($\delta_T \ll L$), the $\delta_C > \delta_T$ assumption means that the concentration boundary layer can be either distinct [$\delta_C \ll L$, case 1.1.b.1] or not distinct [$\delta_C \gg L$, case 1.1.b.2]. Relying on equation (37), we conclude that the criterion that guarantees distinct C layers in case 1.1.b is

$$\frac{L}{H} Le\, Ra_H^{1/2} \gg 1. \tag{38}$$

Case 1.2. When the thermal boundary layers are not distinct, the circulation fills a vertical region of thickness of order L and height H. The scale laws

recommended by the mass and momentum equations in a vertical region of height H and thickness L are

$$\frac{u}{L} \sim \frac{v}{H} \tag{39}$$

$$\frac{v}{L} \sim \frac{gk}{\nu}\left(\beta \frac{\Delta T}{L}\right). \tag{40}$$

These two relations yield

$$v \sim \frac{\alpha}{H} Ra_H \tag{41}$$

$$u \sim \frac{\alpha L}{H^2} Ra_H. \tag{42}$$

It is worth noting that based on scales (41) and (42) the ratio (vertical convection)/(lateral thermal diffusion) in the energy equation (6) is of order

$$\frac{v\Delta T/H}{\alpha \Delta T/L^2} \sim \left(\frac{L}{H}\right)^2 Ra_H. \tag{43}$$

Since case 1.2 is valid when the criterion for distinct thermal boundary layers fails [see equation (32)]

$$\frac{L}{H} Ra_H^{1/2} \ll 1. \tag{44}$$

we learn from the energy scaling (43) that the temperature field in case 1.2 is ruled by conduction. This conclusion is consistent with the defining feature of case 1.2, namely, a side heating effect that penetrates the porous layer entirely.

To determine the thickness of the concentration layer, we refer once more to equation (33) and recognize that a concentration boundary layer may exist even in the absence of a distinct thermal boundary layer: this would happen if $\delta_C \ll L$; therefore, the scale analysis of the concentration field branches off into the following two cases.

(a) $\delta_C \ll L$. When the concentration boundary layer is distinct, equation (34) with $x_{scale} \sim \delta_C$

$$\delta_C \sim H(Le\, Ra_H)^{-1/2} \tag{45}$$

which is the same δ_C scale as in case 1.1.a, equation (35). The validity criterion for equation (45) follows from rewriting $\delta_C \ll L$, hence

$$\frac{L}{H} Ra_H^{1/2} \gg Le^{-1/2} \tag{46}$$

(b) $\delta_C \sim L$. When the concentration boundary layers are not distinct, $\delta_C \sim L$ and the ratio (vertical mass convection)/(lateral mass diffusion) in the constituent conservation equation (7) is of order

$$\frac{v\Delta C/H}{D\Delta C/L^2} \sim \left(\frac{L}{H}\right)^2 Ra_H. \tag{47}$$

The above quantities are considerably smaller than 1 [see equation (44)]; therefore, case 1.2.b is one of pure diffusion.

The scale analysis of heat-transfer-driven flows (class 1) shows that the possible flow regimes occupy well-defined regions in the two-dimensional domain $Le-(L/H)^2\, Ra_H$. Figure 5 is a log–log plot of this domain; on each subdomain are listed the main conclusions of scale analysis regarding the overall heat and mass transfer rates. Note that the order of magnitude of the diffusion-referenced Nusselt and Sherwood numbers defined in equations (20) and (21) are known since the δ_T and δ_C scales have been determined in the

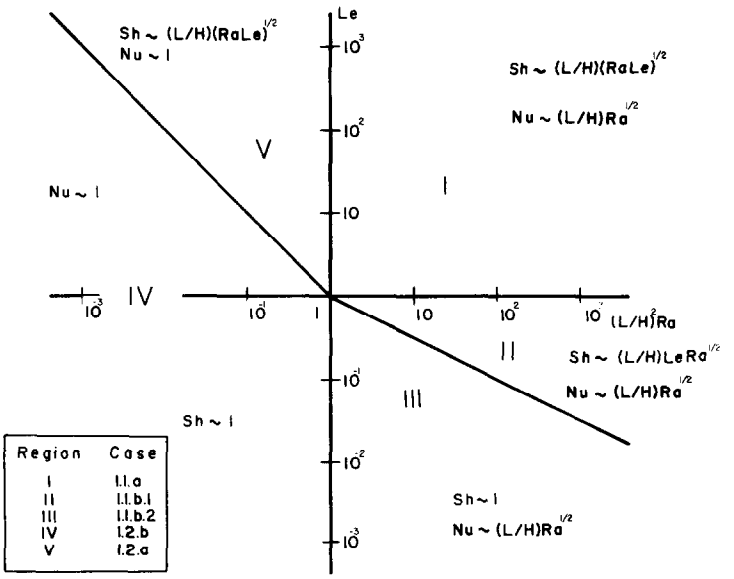

FIG. 5. The flow regimes possible when the buoyancy effect is due mainly to temperature gradients ($|N| \ll 1$).

analysis presented above.

$$Nu = \frac{q'}{kH\dfrac{\Delta T}{L}} \sim \frac{kH\dfrac{\Delta T}{\delta_T}}{kH\dfrac{\Delta T}{L}} \sim \frac{L}{\delta_T} \tag{48}$$

$$Sh = \frac{j'}{DH\dfrac{\Delta C}{L}} \sim \frac{DH\dfrac{\Delta C}{\delta_C}}{DH\dfrac{\Delta C}{L}} \sim \frac{L}{\delta_C}. \tag{49}$$

2. *Mass-transfer-driven glows*

The flows driven by buoyancy due primarily to concentration gradients, $|N| \gg 1$, can be sorted out in an identical way. In the interest of brevity, however, we report only the main conclusions of this second half of the scale analysis by drawing attention to the symmetry properties of the governing equations (4)–(7). These properties indicate that the scales of class 2 flows can be obtained from the scales of class 1 flows through the simple transformation

$$\begin{aligned} \beta\Delta T &\to \beta_C \Delta C \\ \delta_T &\to \delta_C \\ \delta_C &\to \delta_T \\ \alpha &\to D \\ D &\to \alpha \\ \underbrace{Ra_H}_{\text{class 1}} &\to \underbrace{N\, Ra_H\, Le}_{\text{class 2.}} \end{aligned} \tag{50}$$

Figure 6 shows the $Le-(L/H)^2\, Ra_H\, |N|$ plane and the relative position of all the flow regimes possible under class 2. Listed on the same figure are also the scale analysis predictions concerning the overall heat and mass transfer rates, Nu and Sh.

6. DISCUSSION

In this section we bring together the results produced by the two different methods discussed until now, numerical experiments and scale analysis. The objective of this consolidation effort is two-fold, first, to use the numerical experiments in order to verify the validity of the scaling trends predicted via scale analysis and, second, to use the theoretical scaling trends to correlate the discrete numerical information provided by the experiments summarized in Tables 1–3.

As a first test of the validity of scaling results, Fig. 7 shows the numerical results of Table 2 ($N = 0$, $H/L = 1$) plotted as $Sh\, Ra_H^{-1/2}$ vs Le. The data span the Lewis number range 0.01–100 while the Rayleigh number varies from 50 to 4000. The plot shows convincingly that at Lewis numbers greater than one, the scaling law is $Sh \sim (L/H)(Le\, Ra_H)^{1/2}$, which is in agreement with the conclusion reached via scale analysis in case 1.1.a. Figure 7 shows also that the $Le \ll 1$ data obey a different scaling law, $Sh \sim (L/H)\, Ra_H^{1/2}\, Le$, which confirms the mass transfer scaling results corresponding to case 1.1.b. The numerical data that correspond to the regime filling region III in Fig. 5 are also plotted in Fig. 7: they are drawn with the dashed line so as to be distinguishable from the boundary-layer regime data that illustrate the transition from regime 1.1.a to 1.1.b.

The theoretical transition from regimes 1.1.b.1 and

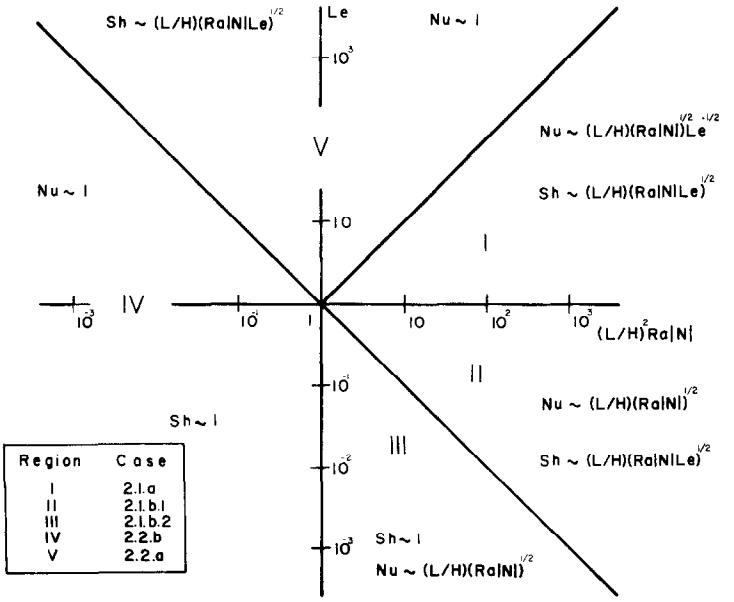

FIG. 6. The flow regimes possible when the buoyancy effect is due mainly to concentration gradients ($|N| \gg 1$).

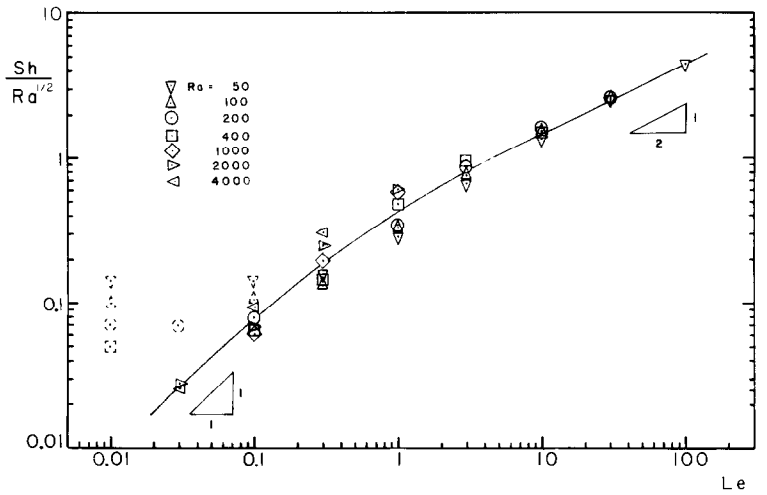

FIG. 7. Correlation of numerical data for regimes 1.1 (a) and 1.1 (b).

1.1.b.2 (regimes II and III in Fig. 5) is tested through numerical experiment in Fig. 8. The ($N = 0$, $H/L = 1$) data of Table 2 are plotted as Sh vs $Le\ Ra_H^{1/2}$. It is evident that if the group $Le\ Ra_H^{1/2}$ is smaller than 1, the Sherwood number is equal to 1, in accordance with transition criterion (38) and the Sherwood number scale (49) (note that when the concentration boundary layers are not distinct, $\delta_C \sim L$, hence $Sh \sim 1$). Figure 8 shows also that when the abscissa parameter $Le\ Ra_H^{1/2}$ exceeds 0(1), the Sherwood number varies as $Le\ Ra_H^{1/2}$.

Recalling the symmetry properties of equations (4)–(7) that led to transformation (50) and Fig. 6, the tests presented in Figs. 7 and 8 validate also the scale analysis of the corresponding regimes of flows driven by mass transfer.

An additional test of the scaling results reported in the preceding section is constructed in Fig. 9. The numerical data of Table 3 are used to show that the Sherwood number of boundary layer mass-transfer-driven flows varies as $(Ra_H\ Le\ |N|)^{1/2}$, in accordance with the scaling results of class 2 phenomena (Fig. 6). Note that in the denominator of the ordinate parameter in Fig. 9, the group $(Ra_H\ Le\ |N+1|)^{1/2}$ was used instead of the group $(Ra_H\ Le\ |N|)^{1/2}$ that was recommended by the scale analysis of $|N| \gg 1$ flows: this slight adjustment is suggested by the flow reversal and convection-suppression effect discovered around $N = -1$ (Fig. 4). Thus, the ratio $Sh/(Ra_H\ Le\ |N+1|)^{1/2}$ is consistently a number of order 1 in the Le range 0.1–100, as N varies from -5 to $+3$. This scaling law holds even for buoyancy ratios in the -1 to 0 range.

In conclusion, the numerical experiments and scale

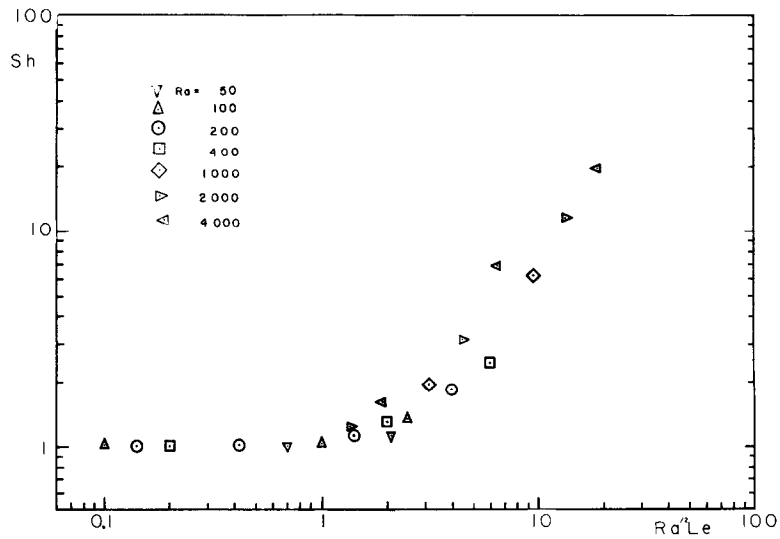

FIG. 8. Correlation of numerical data showing the transition for regime 1.1.b.1 to 1.1.b.2.

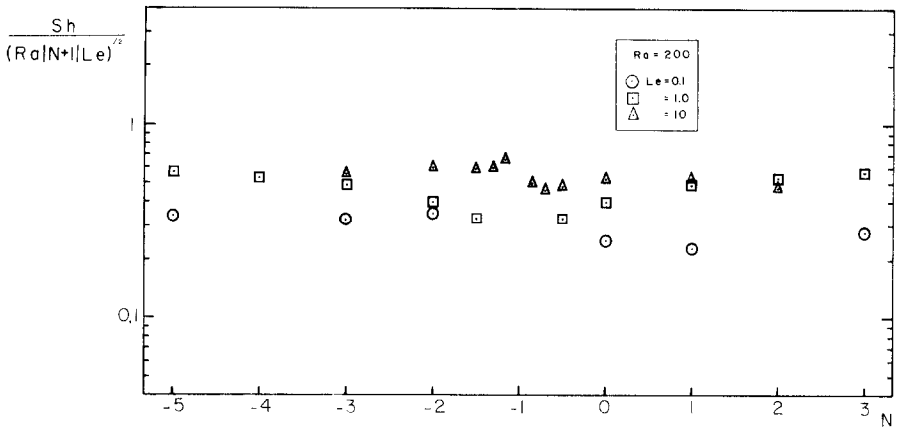

FIG. 9. Correlation of numerical mass transfer results for mass-transfer-driven flows.

analysis of the present study provide a balanced description of the phenomenon of natural convection in a porous layer with combined buoyancy effects. The numerical results support the trends, validity domains and flow regimes predicted by theoretical order-of-magnitude reasoning. The scale analysis, on the other hand, sorted out successfully the many effects that influence the outcome of discrete numerical experiments.

Acknowledgements—Professor O. V. Trevisan wishes to acknowledge the support received from his home institution, Universidade Estadual de Campinas, Brasil. Both authors wish to thank Mr K. R. Blake for the help received in the early stage of the numerical part of this study, and the University of Colorado and Professor M. C. Branch for their hospitality and support of the computational work.

REFERENCES

1. S. Ostrach, Natural convection with combined driving forces, *PhysicoChem. Hydrodynam.* **1,** 233–247 (1980).
2. P. Cheng, Heat transfer in geothermal systems, *Adv. Heat Transfer* **14,** 1–105 (1979).
3. E. R. Lapwood, *Proc. Camb. phil. Soc.* **44,** 508–521 (1948).
4. T. Masuoka, T. Katsuhara, Y. Nakazono and S. Isozaki, *Heat Transfer: Jap. Res.* **7,** 39–52 (1978).
5. R. Rana, R. N. Horne and P. Cheng, Natural convection in a multi-layered geothermal reservoir, *J. Heat Transfer* **101,** 411–421 (1979).
6. R. McKibbin and M. J. O'Sullivan, Onset of convection in a layered porous medium heated from below, *J. Fluid Mech.* **96,** 375–393 (1980).
7. R. McKibbin and M. J. O'Sullivan, Heat transfer in a layered porous medium heated from below, *J. Fluid Mech.* **111,** 141–173 (1981).
8. J. M. Straus, Large amplitude convection in porous media. *J. Fluid Mech.* **64,** 51–63 (1974).
9. J. P. Caltagirone, Thermoconvective instabilities in a horizontal porous layer, *J. Fluid Mech.* **72,** 269–287 (1975).
10. R. N. Horne and M. J. O'Sullivan, Origin of oscillatory convection in a porous medium heated from below, *Phys. Fluids* **21,** 1260–1264 (1978).
11. R. N. Horne and M. J. O'Sullivan, Convection in a porous medium heated from below: the effect of temperature dependent viscosity and thermal expansion coefficient, *J. Heat Transfer* **100,** 448–452 (1978).
12. A. Zebib and D. R. Kassoy, Three-dimensional natural convection motion in confined porous medium, *Phys. Fluids* **21,** 1–3 (1978).
13. J. M. Straus and G. Shubert, 3-D convection in a cubic box of fluid saturated material, *J. Fluid Mech.* **91,** 155–165 (1979).
14. G. Shubert and J. M. Strauss, 3-D and multicellular steady and unsteady convection in fluid-saturated porous media at high Rayleigh numbers, *J. Fluid Mech.* **94,** 25–38 (1979).
15. E. Palm, J. E. Weber and O. Kvernovold, On steady convection in a porous medium, *J. Fluid Mech.* **54,** 153–161 (1972).
16. R. J. Buretta and A. S. Berman, Convective heat transfer in a liquid saturated porous layer, *J. appl. Mech.* 249–253 (1976).
17. P. H. Holst and K. Aziz, Transient three-dimensional natural convection in confined porous media, *Int. J. Heat Mass Transfer* **15,** 73–90 (1972).
18. Y. T. Chan and S. Banerjee, Analysis of transient three-dimensional natural convection in porous media, *J. Heat Transfer* **103,** 242–248 (1981).
19. M. A. Combarnous and S. A. Bories, Hydrothermal convection in saturated porous media, *Adv. Hydrosci.* **10,** 231–307 (1975).
20. J. J. Schneider, Investigation of the influence of free thermal convection on heat transfer through granular material, International Institute of Refrigeration, Proceedings, paper 11-4 (1963).
21. G. Mordchelles-Regnier, P. Micheau, A. Pirovano, C. Jumentier, J. S. Terpstra, Y. Lecourt, P. Cave and M. Breuille, Récherches recentes effectuées en France sur l'isolation thermique des réacteurs nucléaires, International Atomic Energy Agency, Vienna (1969).
22. S. Klarsfeld, Champs de température associés aux movements de convection naturelle dans un milieu poreux limité, *Revue Generale de Thermique* **108,** 1403–1423 (1970).
23. C. G. Bankvall, Natural convection in vertical permeable space, *Wärme-u. Stoffubertr.* **7,** 22–30 (1974).
24. B. K. C. Chan, C. M. Ivey and J. M. Barry, Natural convection in enclosed porous media with rectangular boundaries, *J. Heat Transfer* **92,** 21–27 (1970).
25. P. J. Burns, L. C. Chow and C. L. Tien, Convection in a vertical slot filled with porous insulation, *Int. J. Heat Mass Transfer* **20,** 919–926 (1977).
26. J. E. Weber, The boundary layer regime for convection in a vertical porous layer, *Int. J. Heat Mass Transfer* **18,** 569–573 (1975).

27. A. Bejan, On the boundary layer regime in a vertical enclosure filled with a porous medium, *Letters Heat Mass Transfer* **6,** 93–102 (1979).
28. P. C. Simpkins and P. A. Blythe, Convection in a porous layer, *Int. J. Heat Mass Transfer* **23,** 881–887 (1980).
29. P. A. Blythe and P. C. Simpkins, Thermal convection in a rectangular cavity, in *Physicochemical Hydrodynamics*, Vol. 2, pp. 511–524. Advance, New York (1977).
30. P. A. Blythe and P. G. Simpkins, Convection in a porous layer for a temperature dependent viscosity, *Int. J. Heat Mass Transfer* **24,** 497–506 (1981).
31. K. L. Walker and G. M. Homsy, Convection in a porous cavity, *J. Fluid Mech.* **87,** 449–474 (1978).
32. A. Bejan and C. L. Tien, Natural convection in a horizontal porous medium subjected to an end-to-end temperature difference, *J. Heat Transfer* **100,** 191–198 (1978).
33. C. E. Hickox and D. K. Gartling, A numerical study of natural convection in a horizontal porous layer subjected to an end-to-end temperature difference, *J. Heat Transfer* **103,** 797–802 (1981).
34. D. A. Nield, Onset of thermohaline convection in a porous medium, *Water Resources Res.* **4,** 553–560 (1968).
35. G. Z. Gershuni, E. M. Zhukhovitskii and D. V. Lyubimov, Thermal concentration instability of a mixture in a porous medium, *Sov. Phys. Dokl.* **21,** 375–377 (1976).
36. J. S. Turner and L. B. Gustafson, The flow of hot saline solutions from vents in the sea floor—some implications for exhalative massive sulfide and other ore deposits, *Econ. Geol.* **73,** 1082–1100 (1978).
37. A. A. Khan and A. Zebib, Double diffusive instability in a vertical layer of a porous medium, *J. Heat Transfer* **103,** 179–181 (1981).
38. A. Raptis, G. Tzivanidis and N. Kafousias, Free convection and mass transfer flow through a porous medium bounded by an infinite vertical limiting surface with constant suction, *Letters Heat Mass Transfer* **8,** 417–424 (1981).
39. A. Bejan, *Convection Heat Transfer*, Chap. 9. Wiley, New York (1984).
40. S. Patankar, *Numerical Heat Transfer and Fluid Flow*. Hemisphere, New York (1980).

CONVECTION NATURELLE DUE AUX EFFETS DE TRANSFERT COUPLE DE CHALEUR ET DE MASSE DANS UN MILIEU POREUX

Résumé—On décrit une étude de phénomènes de convection naturelle dans une couche poreuse avec transfert latéral de chaleur et de masse. La circulation naturelle est animée par les effets de pesanteur combinés aux variations de température et de concentration. La première partie de l'étude concerne une série extensive de simulations numériques, dans le domaine $0{,}01 < Le < 100, 50 < Ra_H < 10, -5 < N < +3$ et $H/L = 1$ où Le, Ra_H, N et H/L sont les nombres de Lewis, de Rayleigh–Darcy modifié, le rapport de pesanteur et le rapport de forme de la couche poreuse. Dans la seconde partie, le phénomène est étudié sur la base de l'analyse d'échelle : les conclusions principales, soit les prédictions de l'ordre de grandeur pour les flux de chaleur et de masse et leurs domaines de validité, sont en accord avec les résultats d'expériences numériques discrètes. L'analyse d'échelle est utilisée pour dégager les divers effets qui influencent les résultats globaux de transfert de chaleur et de masse des expériences numériques.

NATÜRLICHE KONVEKTION MIT ÜBERLAGERTEN AUFTRIEBSERSCHEINUNGEN DURCH WÄRME- UND STOFFTRANSPORT IN EINEM PORÖSEN MEDIUM

Zusammenfassung—Diese Arbeit beschreibt eine umfassende Untersuchung der natürlichen Konvektion in einer porösen Schicht mit seitlichem Wärme- und Stofftransport. Die natürliche Zirkulation wird durch Auftriebskräfte hervorgerufen, die durch Temperatur- und Konzentrationsunterschiede hervorgerufen werden. Der erste Teil der Untersuchung enthält zahlreiche numerische Simulationsrechnungen in den Bereichen $0{,}01 \leqslant Le \leqslant 100, 50 \leqslant Ra_H \leqslant 10^4, -5 \leqslant N \leqslant +3$ und $H/L = 1$, wobei Le die Lewis-Zahl, Ra_H die nach Darcy modifizierte Rayleigh-Zahl, N der Auftriebsparameter und H/L das geometrische Seitenverhältnis der porösen Schicht ist. Im zweiten Teil wird das Phänomen ähnlichkeitstheoretisch untersucht: Wichtigstes Ergebnis ist dabei, daß die Berechnung des gesamten Wärme- und Stofftransports und der entsprechenden Gültigkeitsbereiche—mittels Abschätzung der Größenordnungen—gut mit den Ergebnissen der numerischen Untersuchungen übereinstimmt. Weiterhin werden die Ähnlichkeitsbetrachtungen dazu verwendet, die zahlreichen Größen zu erkennen, welche die numerischen Ergebnisse des gesamten Wärme- und Stofftransports beeinflussen.

ЕСТЕСТВЕННАЯ КОНВЕКЦИЯ В ПОРИСТОЙ СРЕДЕ ПРИ УЧЕТЕ ВЛИЯНИЯ СОВМЕСТНОГО ТЕПЛО-И МАССООБМЕНА

Аннотация—В работе всесторонне изучаются явления естественной конвекции, возникающей внутри пористого слоя при тепло-и массообмене на боковой поверхности. Естественная конвекция возникает из-за неоднородной плотности в результате изменения как температуры, так и концентрации. В первой части работы содержится большое количество численных расчетов, проведенных в диапазоне $0{,}01 \leq Le \leq 100$, $50 \leq Ra_H \leq 10^4$, $-5 \leq N \leq +3$ и $H/L = 1$, где Le, Ra_H, и H/L—число Льюиса, модифицированное по Дарси число Рэлея, критерий плавучести и отношение сторон пористого слоя. Во второй части естественная конвекция рассматривается на основе анализа размерностей: основные выводы этой части—оценки порядка величин для коэффициентов общего тепло-и массообмена и определение соответствующих областей применимости—хорошо совпадают с результатами, полученными с помощью выборочных численных расчетов. Более того, анализ размерностей применяется для рассмотрения большого количества эффектов, влияющих на результаты численных расчетов тепло-и массообмена.